Time Dependent Density Functional Theory for Strongly Correlated Systems out of Equilibrium

Master's Thesis
Daniel Karlsson
Division of Mathematical physics, Lund University
November, 2009
Supervisor: Claudio Verdozzi

Abstract

The purpose of this thesis is twofold: i) to present time and space-resolved simulations of the density of trapped ultracold fermions where we switch off the trapping potential in a near-adiabatic, moderately slow and instantaneous manner. The fermions are described using Time Dependent Density Functional Theory, TDDFT, using an exchange-correlation (xc) potential from a 1-dimensional reference system. The out-of-equilibrium dynamics of the Mott insulator is found to differ profoundly from that of the band insulator and the metallic phase, displaying the self-induced stability of the Mott insulator, ii) to propose a new method for obtaining xc-potentials for 3D lattices using Dynamical Mean Field Theory, DMFT. A comparison between this potential from DMFT and the potential obtained from a 1-dimensional system has been made. The time evolution from the different potentials was found to differ, especially when the density was close to half-filling. The xc potential obtained via DMFT is shown, within TDDFT, to be able to describe strongly correlated electrons in presence of time dependent fields, out of equilibrium.

Contents

List of Figures

List of Symbols and Abbreviations

N	Total number of electrons
$N_{\uparrow/\downarrow}$	Number of up / down electrons
L	Total number of sites
c	Electron destruction operator
$c^\dagger$	Electron creation operator
t	Hopping parameter
U	Electron-electron repulsion energy
n	Electron or atom density
$\hat{n}$	Electron or atom density operator
τ	Time
τ_0	Speed of perturbation
φ	Kohn-Sham orbital
ε	Kohn-Sham eigenvalue
v_{KS}	Kohn-Sham effective potential
T	Total kinetic energy
T_0	Non-interacting kinetic energy
E_H	Hartree energy
E_{xc}	Exchange-Correlation energy
v_{xc}	Exchange-Correlation potential
DFT	Density Functional Theory
TDDFT	Time Dependent Density Functional Theory
LDA	Local Density Approximation
ALDA	Adiabatic Local Density Approximation
BALDA	Bethe Ansatz Local Density Approximation
DMFT	Dynamical Mean Field Theory

Chapter 1

Introduction

Understanding solid state physics is not easy. One has to understand the many-body physics for an Avogadro's number, 10^{23}, of particles at the same time. Instead, the paradigm of solid state physicists is to hope that the mutual interactions between the vast number of electrons can be excluded or described at a mean-field level, and perhaps included afterwards in a perturbative manner. This is the independent or mean field electron picture, and the band structure calculations evolving from this picture have been very successful in describing metals and insulators. However, such calculations fail in materials which have strong electron-electron interactions, such as heavy-fermion systems, high T_c superconductors, transition metal oxides, etc. More in general, many materials, for example NiO and V_2O_3, are predicted by conventional band structure calculations to be metals, but in fact they are insulators because of the electron repulsion. Such insulators are called *Mott insulators*, and are still not fully understood.

Thus, there are many circumstances in which electron-electron interactions are important. One way of including such interactions in a material has been Density Functional Theory DFT [1], which describes the physics in terms of densities instead of wave functions. There also exists a time dependent version of DFT, Time Dependent Density Functional Theory TDDFT [2], which is important because a vast fraction of today's research in condensed matter is devoted to non-equilibrium phenomena. The latter are very important, due to their potential importance for technological applications. Time dependent behavior is considerably more difficult to understand than its ground state counterpart, and this reflects in an intrinsic, considerably greater complexity of the inherent theoretical approaches. Ab-initio (methods using no empirical data) TDDFT treatments are rather effective for weakly correlated systems. However, their effectiveness in the case of strong correlations is at present an open problem. Thus, to gain insight, it can be beneficial to study simple model systems.

The theme of this thesis is to use TDDFT on the very popular Hubbard

model. This model is often used to describe qualitative features of systems with a large electron-electron interaction, for example if the material is in an insulating or metallic phase, or how the fermion density distribution look like. Systems like these, with a large electron-electron interaction are commonly referred to as strongly correlated systems. The model is also used in describing the dynamics of cold atoms, trapped in optical lattices. The idea of using TDDFT for the time evolution of the Hubbard model out of equilibrium is quite recent, and was introduced for the first time in 2008 [3].

The strategy in DFT and TDDFT is to group all the troublesome many-body interactions into one quantity, called the exchange-correlation energy, and then approximate this. This energy is then taken to be equal of that of a reference system which nowadays is almost exclusively the homogeneous electron gas, a 3D system in which the effect of the ions in the system is replaced by a constant background, which is referred to as the *Jellium model*. The electron density of such a system is thus constant in space everywhere.

Such a reference system does well in systems where the importance of the electron-electron interactions are low, such as, for example, in Aluminum metal. However, when those interactions are important and differ from an electron gas, the approximation breaks down. This happens for low dimensionality systems, for example in 1D structures or at surfaces (2D). Also, if electrons occupy localized orbitals, the interactions are large and the electron localized at lattice sites, vastly different in behavior from an electron gas. Thus, DFT, and even more so, TDDFT, have a problem in describing strongly correlated systems. One needs to have an energy functional which should approximately give the correct many-body behavior. Thus, the construction of exchange-correlation energies is an active area of research. For example, a key paper in xc-potential development, by Perdew, Burke and Ernzerhof [4], has about 12 000 citations, according to the Web of Science. By contrast, the original, seminal DFT paper by Kohn and Sham has 16 000 citations.

For 1D systems, one can resort to another reference system, called the Luttinger liquid. From this system, Capelle and collaborators [5] have created an exchange-correlation potential, based on the Bethe Ansatz Local Density Approximation (BALDA), which can be used to simulate strongly correlated electrons in 1D. The use of this BALDA in TDDFT was proposed by Verdozzi [3]. A generalization to a spin-dependent formulation was done by Polini and collaborators [6]. Part of this thesis will describe this in more detail, as well as provide results from time evolutions performed in this manner. Thus, for 1D there exist potentials to be used for strongly correlated systems. However, no good reference system exists, to the best of our knowledge, in the case of strongly correlated electrons localized on a three-dimensional lattice.

One very important many-body technique to describe strongly correlated systems is Dynamical Mean Field Theory (DMFT) [7]. This is essentially

an equilibrium method, formulated in terms of Green's functions. Recently, DMFT has been generalized to the time dependent case, but only for very special situations, and it is also very expensive computationally-wise.

While DMFT and TDDFT are nowadays two well established techniques, merging them in a single scheme, where DMFT is used to produce non-perturbative xc-potential to DFT and TDDFT, is completely novel, and it is proposed for the first time in this thesis.

Using these new functionals we can then, by using TDDFT, study density profiles as they evolve in time under the influence of strong correlation effects.

The outline of the thesis is as follows: First is the theory section, which provides more details about BALDA, DMFT and TDDFT in general. Then the main points of the simulation details follow, and here is also the obtained results from these simulations. The results for simulations on cold atoms are presented there, followed by simulations using the TDDFT+DMFT method. Finally, the last section discusses and summarizes these results and provides an outlook for future work in the subject of time dependent density functional theory for strongly correlated systems.

Chapter 2

Theory

2.1 The Model

The model used for all the simulations is the Hubbard model in the presence of an external field. This is a discrete lattice model, which uses a basis set consisting of lattice sites. Due to the Pauli principle, each site can have four configurations: empty, occupied with a spin-up electron, a spin-down electron, or doubly occupied. Each lattice site has a single energy level, the on-site energy. Furthermore, the basis set is assumed to be orthonormal.

The model can be written in second quantization as:

$$\hat{H}(\tau) = -t \sum_{\langle ij \rangle, \sigma} c_{i\sigma}^{\dagger} c_{j\sigma} + \sum_{i} U_i \hat{n}_{i\uparrow} \hat{n}_{i\downarrow} + \sum_{i} v_i \hat{n}_i + V_{ext}(\tau) \tag{2.1}$$

Here t is the hopping parameter, which is the tunneling amplitude between different sites in the system. The amplitude is taken to be equal for all the sites in the system, and in the simulations $t = -1$. Moreover, $\langle ij \rangle$ denotes nearest neighbor sites, meaning that electrons can tunnel only to nearest neighboring sites. $\hat{n}_{i\sigma} = c_{i\sigma}^{\dagger} c_{i\sigma}$, with $\sigma = \uparrow, \downarrow$, is the local density operator expressed in terms of electron creation and destruction operators, whilst $\hat{n}_i = \hat{n}_{\uparrow} + \hat{n}_{\downarrow}$ is the total density operator. The electron-electron interaction is taken to be local (on-site) and is denoted by U_i. The term $\sum_i v_i \hat{n}_i$ is the on-site energy. Finally, $V_{ext}(\tau)$ is the external potential applied to the system in time dependent calculations.

Models such as this one are more directed towards the understanding of the qualitative behavior of strongly correlated systems, than trying to calculate physical properties with good agreement to experiments.

For a more thorough introduction to the Hubbard model, second quantization and exact diagonalization, see my B.Sc. thesis, [8].

2.2 Density Functional Theory (DFT)

The aim of DFT is to reformulate quantum mechanics so that the important object is not the wave function anymore, but the single particle density. In fact, the ground state properties of a system are uniquely determined by the ground state particle density, which was first shown by Hohenberg and Kohn [1].

The theorem states that the kinetic and interaction energy can be written as a functional of n, $F[n]$, and that the total energy can be written as the minimum of $E_v[n] = F[n] + \int vn$. A functional $F[n]$ is a rule F which takes a function $n(r)$ and gives a number $F[n]$ as a result. As an example, the total number of particles N is the functional $N[n] = \int n(r)d^3r$.

The total energy is usually written as a sum,

$$E_v[n] = T[n] + U[n] + \int vn \tag{2.2}$$

where T is the total kinetic energy of the particles in the system, U is the particle-particle interaction, and $\int vn$ is the external potential depending on the system of interest, e.g. a lattice potential or an external perturbation.

It was also shown by Hohenberg and Kohn that the energy in Equation (2.2) is minimal when the density is equal to the ground state density, thus giving the ground state energy.

However, this will only work in principle, because one usually does not know the expressions for the different terms, as expressed in densities. So, to proceed, the terms in Equation (2.2) must be approximated.

To do so, the kinetic energy is usually expressed as $T = T_0 + T_{xc}$ where T_0 is the kinetic energy of a fictitious non-interacting system, $T = \langle\psi|\hat{T}|\psi\rangle$, $|\psi\rangle$ is the many-body wave function, and T_{xc} is the exchange-correlation part of the kinetic energy. In the same spirit, the total interaction U is written as $U = E_H + U_{xc}$, where E_H is the Hartree energy, which is the mean field contribution to the energy, and U_{xc} is the remainder. The total energy is then rewritten as

$$E_v[n] \equiv T[n] + U[n] + V_v[n] = T_0[n] + E_H[n] + E_{xc}[n] + \int vn \tag{2.3}$$

Thus, a new quantity called the *exchange-correlation energy* has been defined, $E_{xc} = T_{xc} + U_{xc}$, which contains the effect of interactions beyond the Hartree level, since the mean field part has been taken out explicitly. The motivation behind this rewriting is that the kinetic energy for the non-interacting system is simply the sum of the kinetic energy for each particle. For the Hubbard model, $\hat{T}_0 = -t\sum_{\langle ij\rangle,\sigma} c^\dagger_{i\sigma}c_{j\sigma}$. The Hartree contribution to the energy is

$$E_H = \frac{1}{4}\sum_i U_i n_i^2 \tag{2.4}$$

Note that this is simply a rewriting, in which all of the correlation and exchange effects are baked into the unknown quantity $E_{xc}[n]$, which is a functional of the density. This is a very complicated object, and finding the exact E_{xc} is , of course, just as hard as finding the exact many-body wave function. The purpose of introducing E_{xc} is to find a suitable approximation to it, and then use this approximation to yield sensible results. The idea is that, since "large" terms such as the Hartree energy has been extracted from it, one can hope that the E_{xc} in some sense will be a 'small' quantity, so that even quite crude approximations to it will bring correct physical results.

To obtain the E_{xc}, one usually finds a reference system, where it is possible to extract the exchange-correlation energy. Then, this E_{xc} is used in the system under study (for example, the paradigm reference system in *ab initio* DFT is the homogeneous interacting electron gas). The trick here is to calculate the total energy E, the single-particle kinetic energy T_0, and then obtain the E_{xc} by

$$E_{xc} = E - T_0 - E_H \tag{2.5}$$

In the end, a functional form for the exchange-correlation energy which can then be used to calculate observables in the system of interest is then obtained.

2.2.1 The Kohn-Sham equations

Practically, Equation (2.3) is not minimized with respect to the energy, but instead one constructs another auxiliary system with density defined to be that of the original system.

In general, under the condition that the integrated density (the total number of particles in the system) is kept fixed, variational derivatives with respect to n are defined only up to arbitrary constants. Thus,

$$C = \frac{\delta E_v[n]}{\delta n(r)} = \frac{\delta T_0[n]}{\delta n(r)} + \frac{\delta E_H[n]}{\delta n(r)} + \frac{\delta E_{xc}[n]}{\delta n(r)} + \frac{\delta \int vn}{\delta n(r)} \tag{2.6}$$

$$= \frac{\delta T_0[n]}{\delta n(r)} + v_H(r) + v_{xc}(r) + v(r) \tag{2.7}$$

where we have defined the Hartree potential $v_H(r)$, the exchange-correlation potential $v_{xc}(r)$ and the external potential $v(r)$. The constant C does not affect the profile of the density variation.

In the Hubbard model, one writes the Hartree potential as

$$v_H(r) \to v_H(i) = \frac{\delta E_H}{\delta n_i} = \frac{\delta}{\delta n_i} \frac{1}{4} \sum_j U_j n_j^2 = \frac{1}{2} U_i n_i \tag{2.8}$$

If we construct an auxiliary, non-interacting system with a single particle potential v_{KS} we get

$$\frac{\delta E_0[n]}{\delta n(r)} = \frac{\delta T_0[n]}{\delta n(r)} + v_{KS}(r) \tag{2.9}$$

Thus, we see that if we want that the same density which minimizes the non-interacting system, Equation (2.9), also minimizes the original interacting system, Equation (2.7), we can choose

$$v_{KS}(r) = v_H(r) + v_{xc}(r) + v(r) \tag{2.10}$$

which means that the ground state density from the full many-body system is the same as for the non-interacting system. Now, for the non-interacting system, we can go from a density representation to a wave function representation, and thus we obtain a Schrödinger-like equation

$$\left(\hat{T} + \hat{v}_{KS}\right) \varphi_i = \varepsilon_i \varphi_i \tag{2.11}$$

where the index i denotes the i-th single particle orbital. Equation (2.11) is called the Kohn-Sham equation, the φ_i are called Kohn-Sham orbitals and v_{KS} is the Kohn-Sham potential.

Since the electrons are independent in the fictional Kohn-Sham system, the ground state is a sum of antisymmetrized products of the orbitals, which can be written as a Slater determinant. The total ground state density is then given by the sum of the squares of the orbitals,

$$n(r) = \sum_{i}^{occ} |\varphi_i(r)|^2. \tag{2.12}$$

which is equal to that of the full many-body system. This ground state will, however, not be a good approximation to the true ground state of the full interacting system.

As in the previous case, in order to solve the problem, one has to find a good approximation to v_{xc}, which is not an easy task. The usual approximation to $v_{xc}(r)$ is to assume a local dependence on the density, that is, the v_{xc} becomes a function of just the density. This is called the Local Density Approximation, LDA. Mathematically, this means

$$v_{xc}[n](r) \approx v_{xc}(n(r)) \tag{2.13}$$

and then one can use the exchange-correlation energy from a reference system to obtain the exchange-correlation potential.

The ground state energy can be calculated once the ground state is known, using (see [9])

$$E = \sum_i^N \varepsilon_i - V_H[n] + E_{xc}[n] - \int n(r) \frac{\delta E_{xc}[n]}{\delta n} d\mathbf{r} \tag{2.14}$$

where the first term is the sum of the Kohn-Sham eigenvalues, the second term is the (subtracted) contribution from the Hartree term, the third term is the exchange energy term, and finally the last (subtracted) term is from the exchange-correlation potential.

We conclude this very brief survey by referring the reader to [9] for a more detailed introduction to DFT.

2.3 Time Dependent Density Functional Theory (TDDFT)

TDDFT is the generalization of DFT to the time dependent case. Non-equilibrium phenomena occupy a central part in today's research, due to their great importance for potential novel technological applications. This is for example the case for nanoscale phenomena, where a small open system (the nanodevice) is in contact with a time-dependent environment. In such nanodevices, usually electron-electron interactions are non-negligible, and this requires a detailed understanding of time dependent correlation effects.

TDDFT is built up from the fundamental theorems from Runge and Gross, [1], which establish a correspondence between time dependent densities and wave functions.

One can, within the framework of TDDFT, also construct a Kohn-Sham (in this case, time-dependent) problem

$$\left(\hat{T} + \hat{v}_{KS}(t)\right) \varphi_i(t) = i \frac{\partial \varphi_i(t)}{\partial t} \tag{2.15}$$

where, similarly to the previous section, one defines

$$n(r,t) = \sum_i^{occ} |\varphi_i(r,t)|^2 \tag{2.16}$$

where the now time-dependent density is equal to the original fully interacting system.

Thus, one evolves the Kohn-Sham orbitals, and obtains the time dependent density $n(r,t)$ in this way. However, the time dependent exchange-correlation potential $v_{xc}[n](r,t)$ is now a much more complicated object than in the ground state scenario. For instance, the exact potential has memory effects, meaning that it is not local in time. For the time dependent case,

one of the most frequently used approximation is the Adiabatic Local Density Approximation, ALDA, which neglects memory effects and non-local dependence on densities. Mathematically, the ALDA states that

$$v_{xc}[n](r,t) \approx v_{xc}(n(r,t)), \tag{2.17}$$

meaning that the exchange-correlation potential depends on the time dependent density only locally, in space and time. One uses the same potential as used in ground state calculations, but replaces the ground state density with the time dependent density.

The important question is: if we want to use DFT and TDDFT for strongly correlated systems, for example for the Hubbard model, how should such a v_{xc} be constructed?

2.4 1D potential: Bethe Ansatz Local Density Approximation, BALDA

The v_{xc}, the exchange-correlation potential from the homogeneous electron gas is built from an infinite system in 3D. One can follow the same procedure for a infinite homogeneous system in 1D, and try to build up an exchange-correlation potential.

As a model Hamiltonian, we use a homogeneous Hubbard model in 1D, which takes the form

$$\hat{H} = -t \sum_{\langle ij \rangle, \sigma} \hat{c}^{\dagger}_{i,\sigma} \hat{c}_{j,\sigma} + U \sum_{i,\sigma} \hat{n}_{i\sigma} \hat{n}_{i,-\sigma} \tag{2.18}$$

Homogeneous in this respect means that the parameters t and U are the same everywhere in the chain. This system can be solved by the Bethe Ansatz, as done by Lieb and Wu [10], and an analytical formula for the total energy density $e = E/L$ is given by, at half-filling (density $n = 1$ everywhere):

$$e^{n=1}(U) = -4 \int_0^{\infty} \frac{J_0(x) J_1(x)}{x(1 + exp(Ux/2))} dx \tag{2.19}$$

where J_0 and J_1 are Bessel functions of the zeroth and first order, respectively.

Based on this exact solution, Capelle and collaborators [5] have shown that one can build up an exchange-correlation potential from this 1D system. This potential will then have the characteristics of a strongly, or weakly, correlated 1D system built in from the beginning, depending on the value of U.

Calulations done with the v_{xc} obtained in the Bethe Ansatz Local Density Approximation (BALDA) have been compared against several other

methods including Quantum Monte Carlo, Density Matrix Renormalization Group etc. and the accuracy for energies and particle densities is generally of the order of a few percent. The advantage of the BALDA is that much larger systems than in most other methods can be treated.

Capelle and collaborators give the following interpolation formula for the total energy density in the case of an infinite homogeneous Hubbard chain in 1D:

$$e^{n\leq 1}(n,U) = -\frac{2\beta(U)}{\pi}\sin\left(\frac{\pi n}{\beta(U)}\right) \tag{2.20}$$

where $\beta(U)$ is determined numerically from

$$-\frac{2\beta}{\pi}\sin\left(\frac{\pi}{\beta}\right) = -4\int_0^\infty \frac{J_0(x)J_1(x)}{x(1+exp(Ux/2))}dx \tag{2.21}$$

Equation (2.20) gives the exact result for $U = 0$ and $U \to \infty$, and is an interpolation formula in between these limits. β takes values between 1 and 2. When $U = 0, \beta = 1$, and when $U \to \infty, \beta \to 2$.

Now, to extract the exchange-correlation energy, one has to subtract the Hartree energy, as well as the non-interacting kinetic energy. Also, it can be shown that the exchange-correlation energy is symmetric around half-filling, $E_{xc}^{n>1}(n) = E_{xc}^{n\leq 1}(2-n)$.

The non-interacting kinetic energy density is given from Equation (2.20) by setting $U = 0$, giving $\beta = 2$,

$$T_0/L = e(n, U=0) = -\frac{4}{\pi}\sin\left(\frac{\pi n}{2}\right) \tag{2.22}$$

The Hartree energy density is given by

$$E_H/L = \langle U\sum_i n_{i\uparrow}n_{i\downarrow}\rangle/L = U\sum_i \langle n_{i\uparrow}\rangle\langle n_{i\downarrow}\rangle/L \tag{2.23}$$

$$= U\sum_i (n/2)^2/L = U\frac{n^2}{4} \tag{2.24}$$

where we are considering the case of an equal amount of up-electrons and down-electrons, so $\langle n_{i\uparrow}\rangle = \langle n_{i\downarrow}\rangle = n/2$ where n is the total density for the uniform system.

Combining everything, we find that $E_{xc}/L = e - T_0/L - E_H/L$, which gives

$$E_{xc}^{n\leq 1}(n)/L = -\frac{2\beta(U)}{\pi}\sin\left(\frac{\pi n}{\beta(U)}\right) + \frac{4}{\pi}\sin\left(\frac{\pi n}{2}\right) - U\frac{n^2}{4} \tag{2.25}$$

$$E_{xc}^{n>1}(n)/L = E_{xc}^{n\leq 1}/L(2-n). \tag{2.26}$$

Finally, taking the derivative of Equation (2.26), $v_{xc} = \dfrac{\delta E_{xc}/L}{\delta n}$, we get the BALDA exchange-correlation potential:

$$v_{xc}^{n\leq 1}(n) = -2\cos\left(\frac{\pi n}{\beta(U)}\right) + 2\cos\left(\frac{\pi n}{2}\right) - U\frac{n}{2} \tag{2.27}$$

$$v_{xc}^{n>1}(n) = -v_{xc}^{n\leq 1}(2-n). \tag{2.28}$$

A plot of the v_{xc} for different values of U is shown in figure 2.1. One can see that for a finite value of U there is always a discontinuity at $n = 1$. Such a discontinuity, however, occurs when the v_{xc} is obtained from an infinite system. For a finite system, the jump at $n = 1$ is expected to be smoothened.

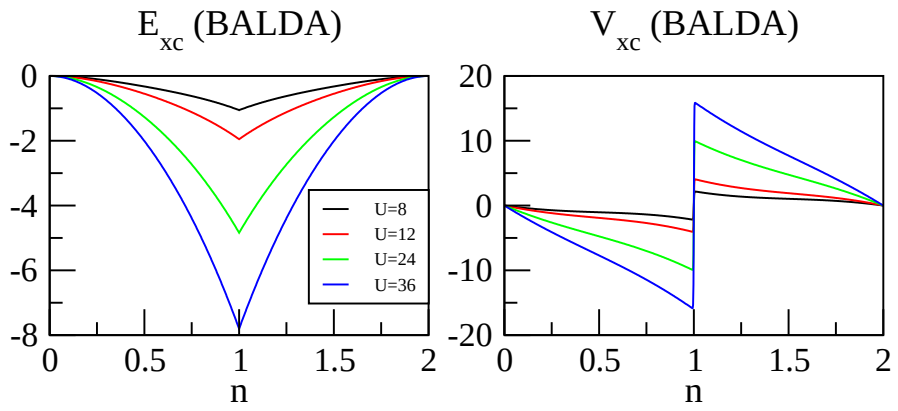

Figure 2.1: *Plot of the BALDA E_{xc} and v_{xc} for different values of U. v_{xc}^{BALDA} always has a discontinuity for $U > 0$ at half-filling, and the gap increases with increasing U.*

2.5 3D potential DMFT, Dynamical Mean Field Theory

The original idea of DMFT first came from W. Metzner and D. Vollhardt [7] in the nineties. They considered the Hubbard model in a lattice with infinite dimensionality, which means that the number of nearest neighbors goes to infinity. The main idea is to focus on a specific lattice site in the homogeneous lattice. In the limit of infinite dimensionality, one can exactly remap the solution of an infinite lattice problem into a single interacting impurity, where the lattice is treated as a reservoir of non-interacting electrons. The impurity site represents one of the sites of the original lattice model (they

are all equal since the system is homogeneous). This new system is then described by the Anderson Impurity Model (AIM), where effective parameters are included to describe the electron bath: [11]

$$H_{AIM} = \sum_{\sigma=\uparrow,\downarrow} \epsilon_0 c_\sigma^\dagger c_\sigma + U c_\uparrow^\dagger c_\uparrow c_\downarrow^\dagger c_\downarrow + \\ + \sum_{\nu\sigma} \epsilon_\nu^{bath} n_{\nu\sigma}^{bath} + \sum_{\nu\sigma} \left[V_\nu c_{0,\sigma}^\dagger a_{\nu,\sigma}^{bath} + V_\nu^\dagger a_{\nu,\sigma}^{\dagger,bath} c_{0,\sigma} \right] \tag{2.29}$$

where $a(a^\dagger)$ is a destruction (creation) operator for a bath of non-interacting electrons in contact with the single site impurity. $c(c^\dagger)$ is the destruction (creation) operator for the impurity. ϵ_ν is the energy of the bath, an effective parameter determined from the original lattice. V_ν is the probability amplitude of adding or removing an electron from the heat bath to the impurity, another effective parameter. The quantities ϵ_0 and U describe the lattice impurity site.

The local impurity site will undergo fluctuations between the four different states: empty, occupied by an up-electron, occupied by a down-electron, and doubly occupied (in this latter case, the two local electrons experience the Hubbard repulsion U). This is schematically shown in Fig. 2.2.

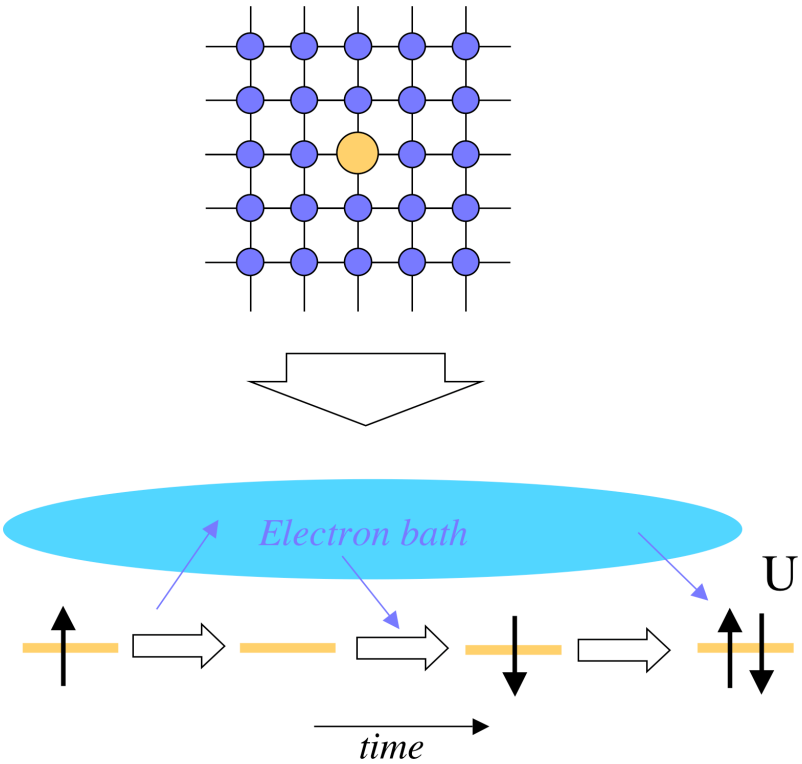

Figure 2.2: *Schematic description of the lattice-to-impurity mapping within DMFT*

In infinite dimensions, the impurity many-body self-energy Σ, which accounts for the interactions among electrons, is local in space (i.e. it has no dispersion in k). This is not true anymore in finite (e.g. $D = 3$) dimensions, but it remains in many cases a good approximation (which is called single-site DMFT). In this case, we can always think of the DMFT as an approach with local self-energy for quantum systems in three-dimensional space. There are also ways to improve such approximation (e.g. cluster DMFT), which could possibly be implemented in future work in this area. In the following we will use single-site DMFT, and expose the general ideas which emerge directly from the treatment in infinite dimensions. Even in this case, the formulation makes use of quite advanced concepts of many-body theory (Green's functions) which are beyond the scope of this thesis. We refer to the original literature for a more detailed presentation [12].

Within the single-site DMFT approach, the on-site Green's function of a homogeneous system, with an equal number of spin-up and spin-down electrons, assumes the form

$$G_H(\omega) = \int_{-\infty}^{\infty} d\omega' \frac{\rho_0(\omega')}{\omega - \omega' - \Sigma_H(\omega')} \tag{2.30}$$

where ρ_0 is the density of states of the free system ($U = 0$), and is the only place in which the structure of the lattice comes in. In the case under consideration this is a simple cubic lattice in three dimensions. The self-energy, as in the case of infinite dimensions, is k-independent.

If we consider now the impurity model, Equation (2.29), the impurity Green's function can be written as

$$G_{imp}(\omega) = \frac{1}{\omega - \epsilon_0 - \Delta(\omega) - \Sigma_{imp}(\omega)} \tag{2.31}$$

where the hybridization function $\Delta(\omega)$,

$$\Delta(\omega) = \sum_{\nu} \frac{|V_\nu|^2}{\omega - \epsilon_\nu^{bath}} \tag{2.32}$$

is determined by the effective parameters of the bath in the impurity model. Thus $\Delta(\omega)$ can be seen as a mean field, [13], but it is frequency-dependent. Thus it is not a *static* mean field, but a *dynamical* mean field.

We want the solution of the impurity model to be that of the original lattice problem. This can be done by requiring that the Green's functions are equal,

$$G_{imp}(\omega) = G_H(\omega) \tag{2.33}$$

which means that the self-energies are also equal,

$$\Sigma_{imp}(\omega) = \Sigma_H(\omega) \tag{2.34}$$

For the Green's function in Equation (2.30) to be equal to the Green's function in Equation (2.31) the following condition must hold:

$$\Delta(\omega) = \omega - \epsilon_0 - \Sigma_{imp}(\omega) - G_H^{-1}(\omega) \tag{2.35}$$

This is the key aspect of single-site DMFT: we are instructing the Anderson impurity model to represent one site of the original lattice model by requiring the local Green's function of the lattice to be identical to the impurity Green's function G_{imp} with identical self-energy. This will impose a self-consistency condition on the shape of the bath surrounding the impurity, whose property is embodied in the function $\Delta(\omega)$. Thus, the parameters ϵ_ν^{bath} and V_ν are varied until self-consistency has been fulfilled.

Due to this mapping between lattice and AIM problem, the entire scheme produces the following iterative procedure: i) start with a guess for Σ_H; ii) solve for the local Green's function G_H; iii) then use Equations (2.33,2.35) to find the hybridization function $\Delta(\omega)$; iv) determine the bath parameters of the effective AIM; v) solve (non-perturbatively) the AIM problem, to find a new self-energy; vi) repeat the cycle until self-consistency.

Once convergence has been obtained, one can extract several quantities from the Green's function. In our case, we want the the kinetic and total energy for a 3D infinite cubic lattice. In a similar way as for the BALDA, one can then obtain a DMFT exchange-correlation energy using the same scheme:

$$E_{xc}^{DMFT} = E_{tot}^{DMFT} - T_0^{DMFT} - E_H^{DMFT} \tag{2.36}$$

where, as before, we subtract the non-interacting kinetic energy and the Hartree energy from the total energy to get the exchange-correlation energy.

Taking the derivative with respect to the density yields the exchange-correlation potential v_{xc}^{DMFT}.

The exchange-correlation potentials and energies obtained from DMFT for homogeneous simple cubic lattices are shown in figure 2.3. Details of the fitting are shown in appendix A.

The physics of the v_{xc} gap

One important characteristic here is to see that while the 1D v_{xc} always has a gap for $U > 0$, for the 3D Hubbard model the v_{xc}^{DMFT} has a gap only when U is above a certain value, which is approximately $U \approx 13t$. This marks a transition from a metal-like behavior to an insulating one, called the Mott transition. In 3D, this transition happens at a finite value of U. Conversely, in 1D, correlation between electrons are much more pronounced, and therefore, at half-filling, a linear chain is always a Mott insulator when $U > 0$ [10].

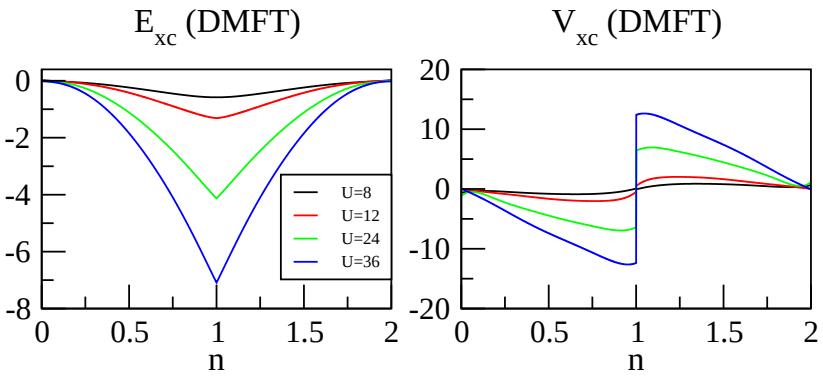

Figure 2.3: *Plot of the DMFT v_{xc} for different values of U. v_{xc}^{DMFT} has a gap when $U > 13$, approximately. The gap increases with increasing U.*

Chapter 3

Simulations

Here the methods used to calculate energies and densities are presented. Also, further down the results for such simulations are shown.

3.1 Methods

This section contains details about how the simulations was made. The DFT calculations as well as the TDDFT calculations were done with a program written by me using Fortran 90.

The exact calculations which were used to compare my DFT and TDDFT results comes from a program written by Claudio Verdozzi.

The Dynamical Mean Field Theory data, which was used to construct the DMFT v_{xc}, was produced by Antonio Privitera using a DMFT impurity solver.

3.1.1 Ground State Calculations

In order to calculate ground states, we solve the single-particle Kohn-Sham equations,

$$\left(\hat{T}_0 + \hat{v}_{KS}\right)\varphi_i = \varepsilon_i \varphi_i$$

The goal is to diagonalize the Hamiltonian $\hat{H} = \hat{T}_0 + \hat{v}_{KS}$, which will give us the Kohn-Sham orbitals φ_i and the Kohn-Sham eigenvalues, ε_i. The ground state for this system is then a Slater determinant consisting of Kohn-Sham orbitals, since the electrons in the fictional system are independent from each other. Once the ground state has been found, one can then calculate various ground state quantities, for instance energy and density.

However, to obtain the Hamiltonian is not straightforward, since $v_{KS}(n)$ is a function of the density. This means that one has to solve the Kohn-Sham equations using a self-consistent scheme. The scheme used is described below.

1) Choose a starting density, preferably a density which fulfills $\sum_i n_i = N$. Our choice was $n_i = n = N/L$ for simplicity, which is the number of electrons divided by the number of sites.

2) Calculate v_{KS} according to Equation (2.10) using the density from the previous step.

3) Diagonalize the Hamiltonian $H = T + v_{KS}$, which will yield the Kohn-Sham orbitals φ_i and the Kohn-Sham energies ε_i.

4) Calculate the new density $n_{new} = \sum_i^{occ} |\varphi_i|^2$

5) Compare n_{new} and n_{old}. If they are equal within a chosen interval, convergence has been reached. If they are not equal, go to 2) with another density n'.

The new density n' can be set to be n_{new}. However, if one requires a high numerical accuracy, such a choice will usually lead to an unstable behavior where the density oscillates around the correct density with each iteration. To solve this, we used a linear blending of densities, which means that only a small part of the new density is used in the next iteration,

$$n' = \alpha n_{new} + (1 - \alpha) n_{old}, \tag{3.1}$$

where $0 < \alpha < 1$. Typically, a lower α means a more stable, but slower, convergence, and we used $\alpha = 0.1$. One can also use more advanced schemes, in which the densities from earlier iterations play a role, as in Broyden or Anderson interpolation [14].

When convergence has been reached, we have the ground state density, and the ground state wave function to the fictional Kohn-Sham system, which is a Slater determinant of Kohn-Sham orbitals. We can also calculate the ground state energy from Equation (2.14).

Convergence issues

There can be systems for which it is very difficult to achieve convergence in ground state calculations. Cases occurred in which the self-consistent calculations never converged, for neither v_{xc}^{BALDA}, v_{xc}^{DMFT} or even putting $v_{xc} = 0$. We have plans to theoretically investigate how to overcome this technical difficulty in the future.

Also, for densities close to half-filling one can also run into problems if the v_{xc} has a discontinuity; the density can tend to oscillate around $n = 1$ in the self-consistency loop. The discontinuity can also cause problems for the time evolution, see below. Therefore, we introduce a smoothing procedure for the v_{xc}. The exchange-correlation potential can be written as

$$v_{xc}(n) = \theta(1 - n) v_{xc}^{n<1}(n) + \theta(n - 1) v_{xc}^{n>1}(n) \tag{3.2}$$

where $\theta(x)$ is the Heaviside step function. We now replace the step function

with a Fermi function,

$$\theta(x) \to F_S(x) = \frac{1}{1+e^{-x/S}}. \tag{3.3}$$

When $S \to 0, F_S(x) \to \theta(x)$. Thus S is the smoothing parameter, and we choose $S = 0.01$ in all the calculations in this thesis. The smoothed exchange-correlation potential now has the form

$$v_{xc}^S(n) = F_{0.01}(1-n)v_{xc}^{n<1}(n) + F_{0.01}(n-1)v_{xc}^{n>1}(n) \tag{3.4}$$

The shape of the smoothed potentials are shown in figure 3.7.

3.1.2 Time Evolution

To time evolve the Kohn-Sham Slater determinant is the same as to time evolve all the Kohn-Sham orbitals. The wave function at a later time is then the Slater determinant of the time evolved orbitals. This means that the density at site j and time τ is given by

$$n_j(\tau) = \sum_i^{occ} |\varphi_i(j,\tau)|^2 \tag{3.5}$$

The method of choice for the time evolution was a split operator scheme. By writing $H(\tau) = T + V(\tau)$, one can split the time evolution operator into a product of exponentials:

$$e^{-iH(\tau)d\tau} = e^{-i(T+V(\tau))d\tau} = e^{-iV(\tau)d\tau/2}e^{-iTd\tau}e^{-iV(\tau)d\tau/2} + O(d\tau^3) \tag{3.6}$$

where $O(d\tau^3)$ contains higher order commutators. The splitting is exact if the two operators T and $V(\tau)$ commute.

In order to time evolve, the kinetic energy is written as $T = ZDZ^\dagger$, where Z is a unitary matrix and D is a diagonal matrix. Also, one uses the fact that $e^{ZDZ^\dagger} = Ze^DZ^\dagger$. This will give us the time propagation formula:

$$e^{-iH(\tau)d\tau} = e^{-i(T+V(\tau))d\tau} = e^{-iV(\tau)d\tau/2}Ze^{-iDd\tau}Z^\dagger e^{-iV(\tau)d\tau/2} + O(d\tau^3) \tag{3.7}$$

The main advantage is that we need to diagonalize T only once, since it is time independent. Furthermore, $V(\tau)$ contains only diagonal elements, so $e^{-iV(\tau)d\tau}$ is also diagonal and can be readily obtained. All the exponentials are now known, and one can time propagate via computationally cheap matrix multiplications.

Thus this is a faster procedure than a simple diagonalization procedure, where a diagonalization at each time step is required.

The convergence, with respect to time, was checked by first running a simulation with timestep $d\tau$, and then another with timestep $d\tau/2$, and then checking that the same results are obtained. Since it is hard to obtain convergence when dealing with discontinuities, a smoothing procedure is necessary here.

Predictor-Corrector

As a further ingredient, we use a Predictor-Corrector algorithm to time propagate. We first propagate in time from τ to $\tau + d\tau$ using the split operator method, with a Hamiltonian called H_{pred}. This is called the predictor step. The new density from the time propagated wave function is then calculated, as well as the new Hamiltonian, H_{corr}, corresponding to this density. This is the corrector step. Now we combine the two Hamiltonians, and take the average of them.

$$H_{pred-corr} = \frac{H_{pred} + H_{corr}}{2} \tag{3.8}$$

The new Hamiltonian $H_{pred-corr}$ is then used to propagate the wave function from τ to $\tau + d\tau$.

3.2 BALDA simulations

We now want to use the 1D exchange-correlation potential obtained in the previous section, to time evolve a specific case, namely ultracold fermions in an optical lattice. An optical lattice is created by counterpropagating laser beams, which produce a stationary interference pattern. This, in turn, offers an optical potential landscape to cold atoms. The space pattern of the landscape optical potential can be tailored, for example, to mimic the profile of a tight-binding lattice. Ultracold fermions in such lattices can be modelled by a Hubbard model. In addition to the Pauli exclusion principle, the physics of such systems is governed by three distinct energy scales: the kinetic energy of the fermions, the potential energy due to the confining trap potential, and the fermion-fermion interaction energy. Various numerical and analytical techniques predict that this interplay gives rise to a characteristic spatially varying density profile, displaying coexistence of metallic, Mott-insulator and band-insulator-like regions in different parts of the trap. Very recently, evidence for such phase-separated density profiles in three-dimensional fermion gases has been obtained experimentally. [15, 16].

Most of such investigations have been directed at the *stationary states* of the many-fermion system, because of the similarity to the possible ground states of strongly-correlated many-electron systems in condensed-matter physics. Optical realizations of trapped fermions on a lattice, however, also allow one to study the *time evolution* of such systems, much more directly and easily than in solid-state experiments, and in great detail. Specifically, we study the time evolution of the characteristic Mott insulator, band-insulator and metallic phases after rapid, moderate or near-adiabatic switching off of the trapping potential. This allows us to address two fundamental problems of many-body physics: '*How does an out-of-equilibrium Mott insulator behave?*' and '*how does the time evolution of a Mott insulator differ*

from that of a band insulator and of a metallic phase'? To answer these questions we present numerical predictions of the out-of-equilibrium density profiles corresponding to the distinct states realized in the trap.

We describe the trapped fermions with the Hamiltonian $\hat{H}(\tau) = \hat{H}_0 + \hat{V}_{ext}(\tau)$:

$$\hat{H}_0 = -t \sum_{\langle ij \rangle, \sigma} c^\dagger_{i\sigma} c_{j\sigma} + U \sum_i \hat{n}_{i\uparrow} \hat{n}_{i\downarrow} + \sum_i v_i \hat{n}_i, \tag{3.9}$$

$$\hat{V}_{ext}(\tau) = -a(\tau) \sum_i v_i \hat{n}_i. \tag{3.10}$$

where the on-site energy builds up the parabolic trap potential $v_i = 0.5k\,(i - i_0)^2$, where i_0 is the center of the system, and k is the spring constant. The on-site interaction is set to be equal everywhere, $U_i = U$.

The external potential $\hat{V}_{ext}(\tau)$ controls the switching off of the parabolic potential via $a(\tau)$, which has the boundary conditions $a(0) = 0$ (unperturbed parabola) and $a(\tau \to \infty) = 1$ (completely switched off parabola). $\hat{n}_i = \hat{n}_\uparrow + \hat{n}_\downarrow$ is the total density operator. In the simulations below, $a(\tau)$ was chosen to be

$$a(\tau) = \begin{cases} \sin\left(\frac{\pi}{2}\frac{\tau}{\tau_0}\right) & \tau < \tau_0 \\ 1 & \tau > \tau_0 \end{cases} \tag{3.11}$$

where the parameter τ_0 controls the speed of the removal of the trap.

A system of 60 fermions on 100 sites with periodic boundary conditions (i.e. a ring) was used. At $\tau < 0$, the fermions were trapped within the parabolic potential with a spring constant of $k = 0.05$. The fermion-fermion interaction was $U = 8$ and the hopping parameter was $t = -1$.

3.2.1 Ground State Calculations using BALDA

The ground state of the system was calculated by solving the Kohn-Sham equations, as described above, and the resulting ground state density is shown in figure 3.1. The ground state density is a result from the struggle between the parabolic potential and the particle interaction; The atoms tend to keep themselves in the middle of the chain to minimize the energy penalty from the parabola, while the particle interaction tends to spread the atoms apart. Also in effect is the Pauli exclusion principle, which also prohibits the fermions from crowding at one place.

In the middle of the chain, the (B) plateau has a density of $n = 2$. The sites are fully occupied with a spin-up and a spin-down fermion, because of the non-existence of the parabolic potential. Since the sites are full, the fermions have an insulating behavior.

The Mott plateaus (M) have an integer value of the density. This is because of the fermion-fermion interaction; there is one fermion on every site, and thus the repulsion U prevents double occupation. This means

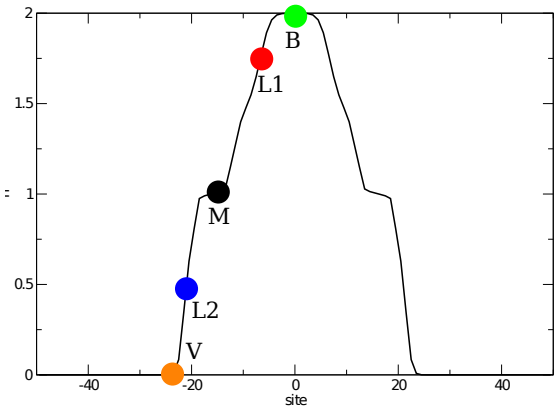

Figure 3.1: *The ground state density as a function of site label, where the origin is at the center of the parabolic potential. The plateaus at $n = 1$ (M) are called Mott plateaus. The plateau at $n = 2$ (B) is the band insulator phase. (V) is outside of the confined fermions, vacuum. The areas (L1) and (L2) are Luttinger regions. The symbols and colors in this figure are also used in the results for the time evolution in the next section.*

that the fermion-fermion interaction induces an insulating behavior. This behavior, or phase, is called a Mott insulator phase. The Mott insulator is therefore fundamentally different than a band insulator; the former is an insulator because of the particle interaction, while the latter is an insulator because of a filled band.

The regions between the plateaus (L) at $n = 1$ and $n = 2$ has the behavior of a Luttinger liquid, which is a 1-dimensional feature, which does not exist in higher dimensions. For more information on such liquids, see [17]

Outside of the vacuum region (V) the parabolic potential is too strong compared to the fermion-fermion repulsion, so the density is negligible there.

3.2.2 Time Evolution using BALDA

At $\tau = 0$ the system in the preceding section was subjected to an external perturbation, the purpose of which was to remove the parabolic trap. This was done for three different speeds of the perturbation. We denote the slowest of these removals as adiabatic removal, and refer to the other two as intermediate and fast. Adiabatic in this respect means that the time evolved state at a time is close to the ground state, which is obtained by using the potential at that same time. The results are shown in the three figures below, figure 3.2, 3.3 and 3.4. As can be seen in the time evolution, the regions behave differently under the perturbation. The band insulator loses its structure immediately as the perturbation change. This is fundamentally

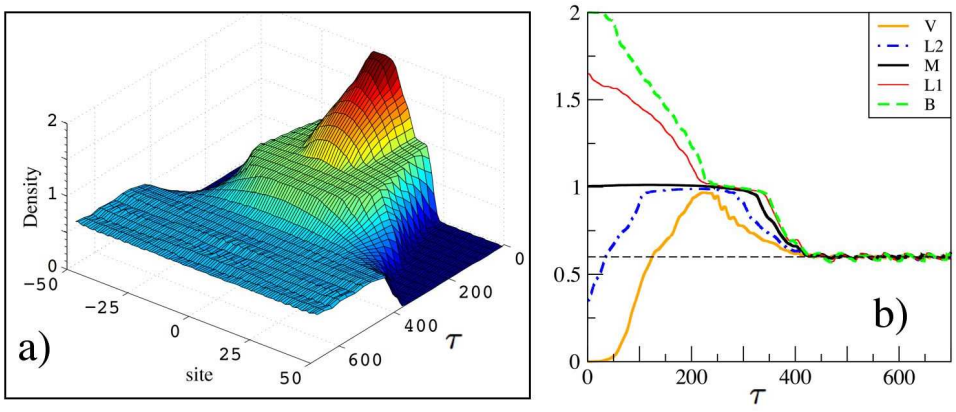

Figure 3.2: *Time evolution using an adiabatic removal of the trap, $\tau_0 = 460$. a) shows a 3D plot of the time evolved density for each site along the chain. b) shows a 2D graph for the densities at the specific sites depicted in figure 3.1. Note how the density from (B), the band insulator, goes down immediately, while the Mott plateau is very stable against the perturbation. The Mott plateau also increases in width over time. The density tends to that of an unperturbed system as $\tau \to \infty$, $n = 60/100 = 0.6$. Because of a finite τ_0, there are still oscillations around 0.6.*

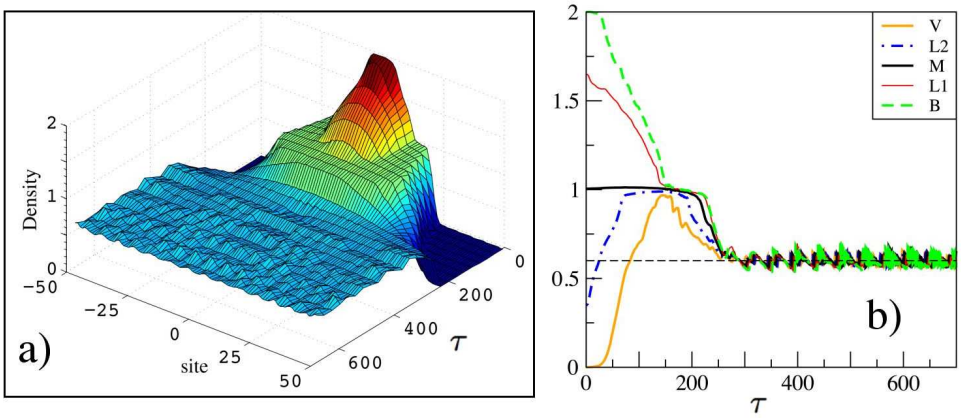

Figure 3.3: *Time evolution using an intermediate speed of the removal of the trap, $\tau_0 = 300$. a) shows a 3D plot of the time evolved density. b) shows a 2D graph for the sites depicted in figure 3.1. The end result is similar to the adiabatic case, figure 3.2, but with more oscillations in end of the simulation.*

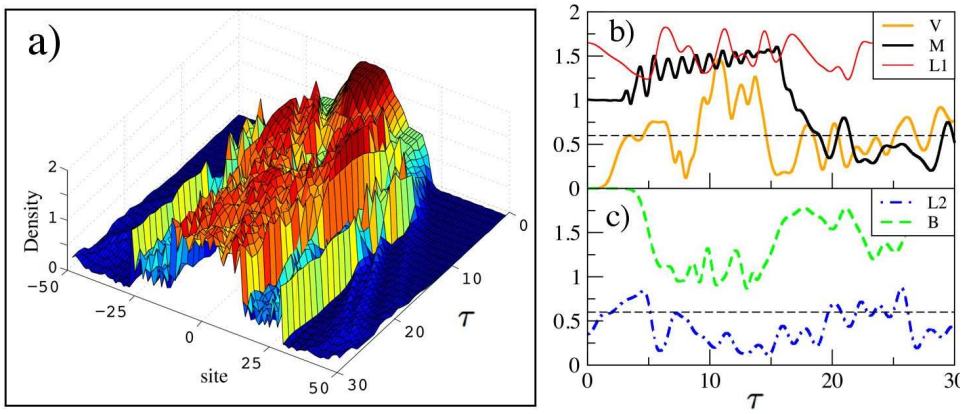

Figure 3.4: *Time evolution using a step-like removal of the trap, $\tau_0 = 0^+$. a) shows a 3D plot of the time evolved density. b) and c) shows a 2D graph for the sites depicted in figure 3.1. This is far away from adiabaticity, and thus the system does not evolve towards constant density as $\tau \to \infty$. Since the system is isolated and finite, the fermions will continue to oscillate in time.*

different from the Mott plateaus, which seems resistant to the change in potential. The Luttinger regions seem to change rather fast, until they reach the Mott plateau, where they are stable for a while. This is called the adiabatic speed, since it is close to the adiabatic limit. This is seen because the density tends to the density of the uniform system, which means that the density is equal to $n = N/L$ everywhere. As the potential goes away faster, the system does not have time to adjust to the external perturbation, and therefore oscillates more rapidly around the uniform density value. This pattern is common to all the kinds of perturbations we investigated. We have checked that this behavior is consistent within a wide range of parameters, and also for larger traps. For more information, see [18].

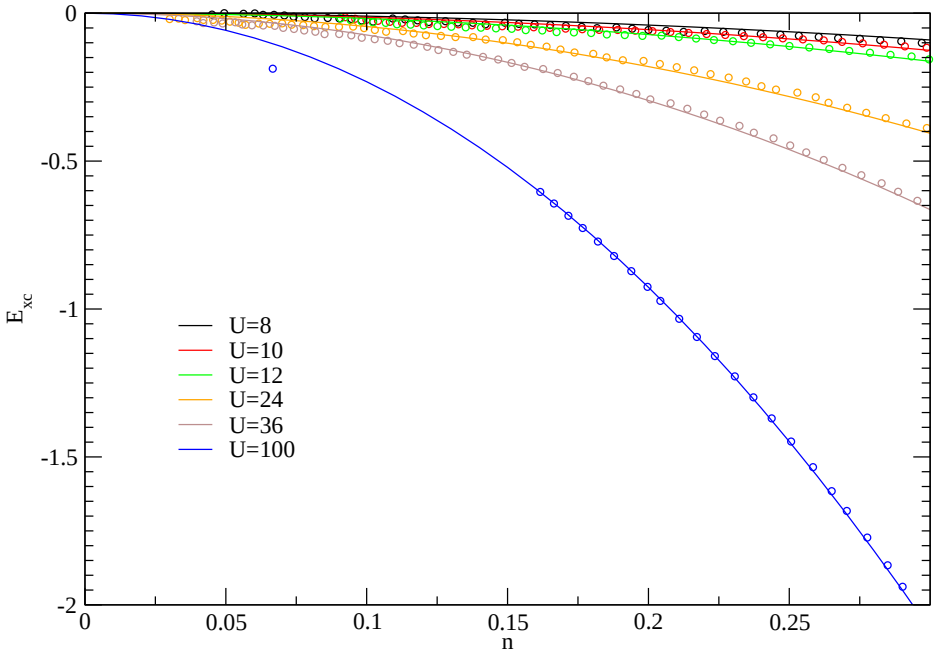

Figure 3.5: *Plot of the xc-energy from the raw data of the DMFT impurity solver (circles) for different values of U, and the corresponding analytical expression by Giuliani (lines) in the case of an infinite homogeneous simple cubic system, plotted as a function of density. The results agree in the low density limit.*

3.3 DMFT simulations

In this section, we leave the 1D systems, and move to the 3D case. We will use the exchange-correlation potential E_{xc}^{DMFT} obtained from the Dynamical Mean Field Theory calculations in section 2.5.

We start our analysis for the E_{xc}^{DMFT}, by checking that the xc-energy has the correct behavior in the low density regime. This is done by comparing the energy to an asymptotic analytical formula given by Giuliani [19], which gives an upper bound of the energy in the low density limit. The result is shown in figure 3.5, where one can see that, in the low density limit, the Giuliani formula and the E_{xc}^{DMFT} agree well. See appendix A for more information.

3.3.1 Ground State Calculations using DMFT

To see if the functionals reproduce the correct ground state energies, we apply DFT using the BALDA and the DMFT v_{xc} and calculate the total energy for different fillings. A homogeneous simple cubic lattice with periodic boundary conditions was used. The results are shown in figure 3.6. For small clusters neither BALDA or DMFT-DFT reproduce the DMFT

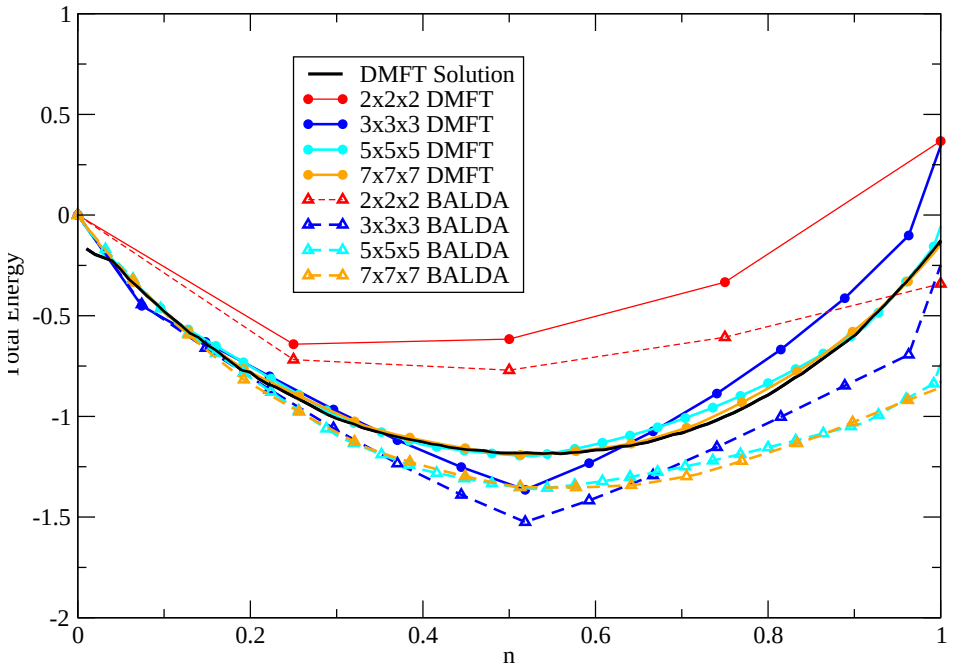

Figure 3.6: *Plot of total energy for homogeneous cubic systems with $U = 24$. The black curve is the raw data from the DMFT impurity solver for an infinite homogeneous lattice. The curves denoted BALDA and DMFT are obtained from DFT calculations, using a BALDA and a DMFT functional, respectively. The geometry was a simple cubic lattice with periodic boundary conditions, where the size of the clusters are given in the legends. When the size of the cube is increased, the DMFT functional produces the correct ground state energy. The BALDA functional does not, and this is because of the differences between the functionals at half-filling, $n = 1$, see figure 3.7.*

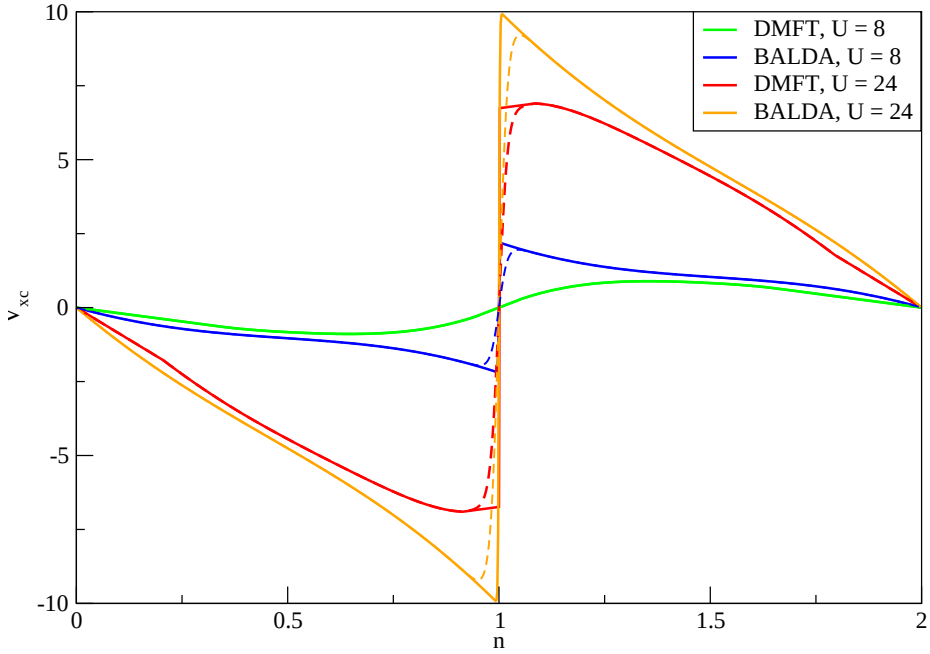

Figure 3.7: *Plot of the DMFT and BALDA v_{xc} for $U = 8$ and $U = 24$. The solid lines are the v_{xc}'s obtained from the methods described in the theory section. The dashed lines are the smoothed v_{xc}'s described above, which were used in the simulations. Although the DMFT and BALDA shapes overall resemble each other, significant differences can be seen: i) The discontinuity opens only for large U in the DMFT case. In fact, this happens when $U > 13$. ii) $|v_{xc}^{BALDA}| > |v_{xc}^{DMFT}|$ always, especially at higher U, and closer to half-filling.*

solution. However, when the size of the cluster is increased, DMFT-DFT obviously converges to the DMFT solution. BALDA, however, does not do this, especially not close to half-filling. The reason for this is the difference in the v_{xc}, see figure 3.7.

3.3.2 Time Evolution using DMFT

We now want to test our new exchange-correlation potential v_{xc}^{DMFT} by comparing TDDFT-simulations to the exact method described in the beginning of the chapter. We consider a system and time evolve it using i) the potential from DMFT v_{xc}^{DMFT}, ii) the potential from BALDA v_{xc}^{BALDA}, iii) the Hartree term only, putting $v_{xc} = 0$, iv) the exact code.

To this end, we consider a $3 \times 3 \times 3$ cube, but with the 8 corners cut off, giving a 19 site cluster, see figure 3.8. We place an impurity with a particle-particle interaction U in the central site, and we put $U = 0$ everywhere else. In the time evolution, the number of spin-up electrons and

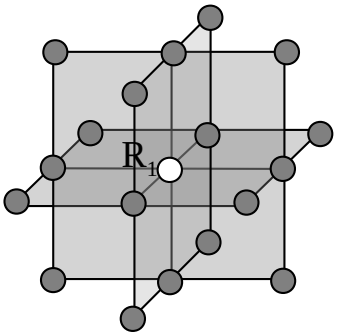

Figure 3.8: *The $3 \times 3 \times 3$ cube with the 8 corners cut off. R_1 is in the center of the cluster, and has an impurity with a particle interaction U. At all other sites, $U = 0$. A time dependent external perturbation is applied to R_1 only, and the time dependent density for this site for various parameters are shown in the graphs below in this section.*

spin-down electrons are the same, $N_\uparrow = N_\downarrow = 3$. Note that this already gives a configuration size $\binom{19}{3}^2 \sim 10^6$ for the exact calculation (modifying the exact diagonalization code to implement the case $N_\uparrow = N_\downarrow = 4$ is in progress). In the figures below, the black curve corresponds to the exact solution, done with a pre-existing code. The red curve corresponds to a density, time evolved using the exchange-correlation potential extracted from the DMFT solution, and the blue curve corresponds to the BALDA potential. We wish to remark that, conceptually, the use of BALDA in 3D is unjustified. However, it is interesting to consider also this approximation to investigate the role of dimensionality on the xc-potential.

In the calculations shown here, we apply a time dependent external perturbation to the middle site only. Two types of perturbations were used,

$$V_{ext}(\tau) = A\sin(\tau), \quad V_{ext}(\tau) = Ae^{-\frac{(\tau-\tau')^2}{\tau_0}}, \tag{3.12}$$

a sinusoidal and a gaussian perturbation where A is the strength, τ' is the mid-point of the gaussian, and τ_0 controls the degree of adiabaticity.

The on-site energy E of the site in the middle was also changed, to control the ground state density. The values are given in the figures below. In all the graphs in this section, the density shown is the density for the middle site.

In figure 3.9, the density in the middle site oscillates back and forth, in phase with the sinusoidal perturbation. This points to the fact that we are using a slowly varying, adiabatic, perturbation. At low densities, any potential (DMFT, BALDA, or Hartree), is in good agreement with the exact solution. However, as the density increases at the central site, we see that the

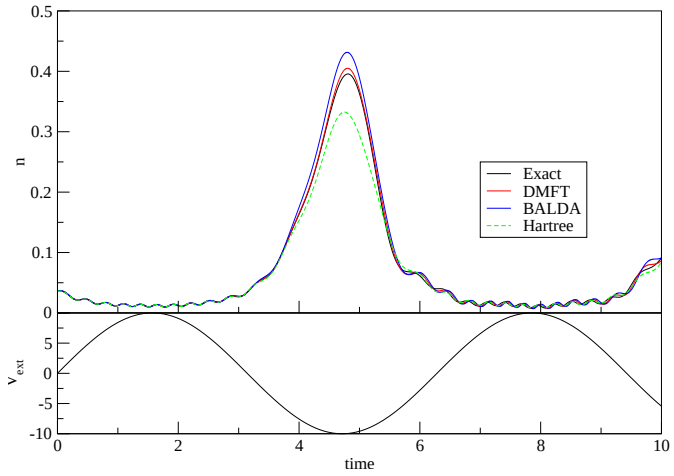

Figure 3.9: *Above: Density of the middle site R_1 as a function of time with the parameters $U = 8, E = 10$. Below: Perturbation as a function of time, $V_{ext}(\tau) = 10\sin(\tau)$.*

DMFT curve is in good agreement, while BALDA overshoots. The Hartree solution, on the other hand, produces a low density.

In figure 3.10, the same behavior as in figure 3.9 can be seen; BALDA is above the exact solution, Hartree is below, and DMFT is above, but closer than BALDA to the exact solution. The exchange-correlation potential is more important in this simulation, since the interaction strength U is larger. This is consistent with the fact that the Hartree density is further away from the exact solution for larger U. In figure 3.11, the perturbation is weaker than in the last two figures, and thus the density is not affected as much as before. The same tendencies as before can be seen, and DMFT is in good agreement here as well.

In figure 3.12, we see that increasing U has the same effect here as before; the xc-potential is more important, and thus the Hartree density is more off from the exact solution, compared to the previous case, in figure 3.11.

In figure 3.13, we can see that, independent of the exchange-correlation potential used, all the densities are the same when the gaussian is at its peak. The explanation for this is that the interaction energy is small in comparison to the external potential, and thus the densities are almost the same. This behavior has been seen also in other simulations, when the density is close to $n = 2$. In figure 3.14, the densities are still similar at the peak of the gaussian, but less so than in figure 3.13. This is because the interaction energy has been increased by a factor of 3.

In figure 3.15, both BALDA and DMFT fit reasonably to the exact solution up to a point, around $t = 4$, when the BALDA solution starts to oscillate, while DMFT does not. The oscillations happen around $n = 1$,

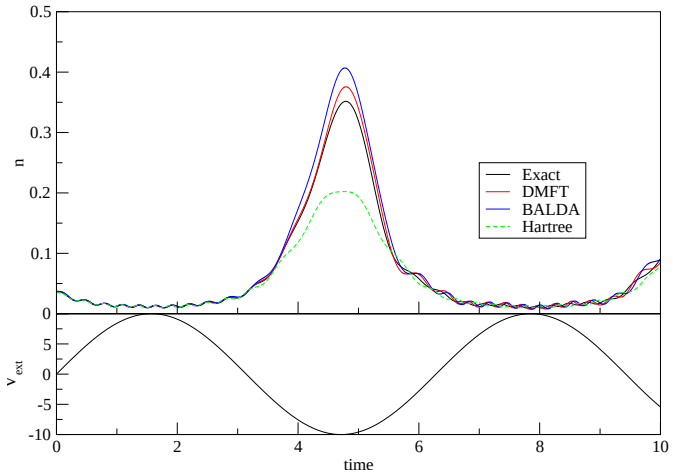

Figure 3.10: *Same as in figure 3.9, but here* $U = 24$.

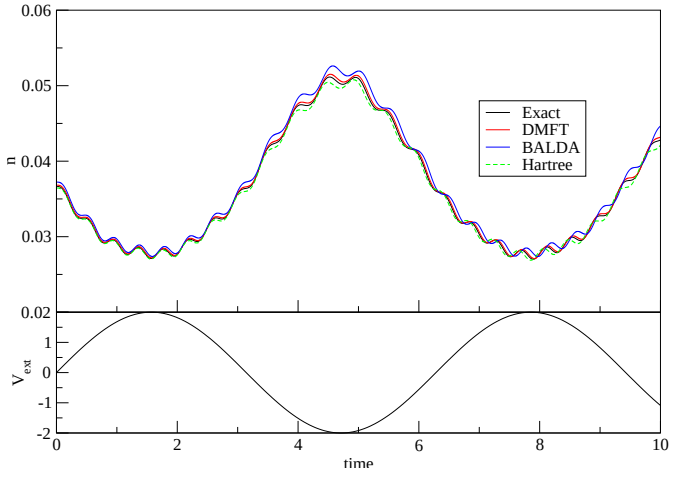

Figure 3.11: *Same as in figure 3.9, but with a weaker external perturbation,* $V_{ext}(\tau) = 2\sin(\tau)$.

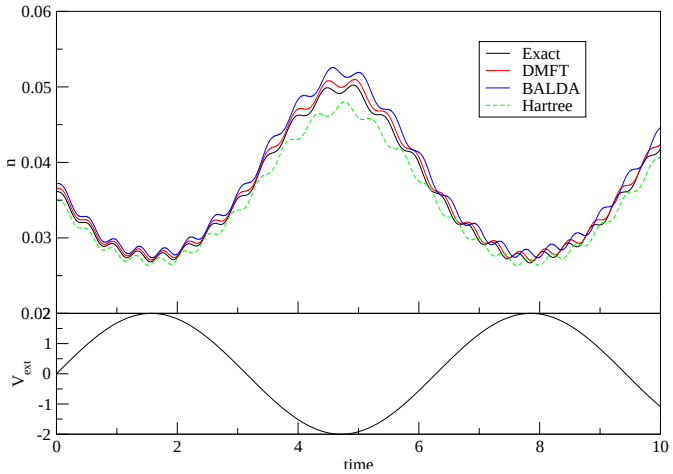

Figure 3.12: *Same as in figure 3.11, but here with a stronger particle interaction,* $U = 24$.

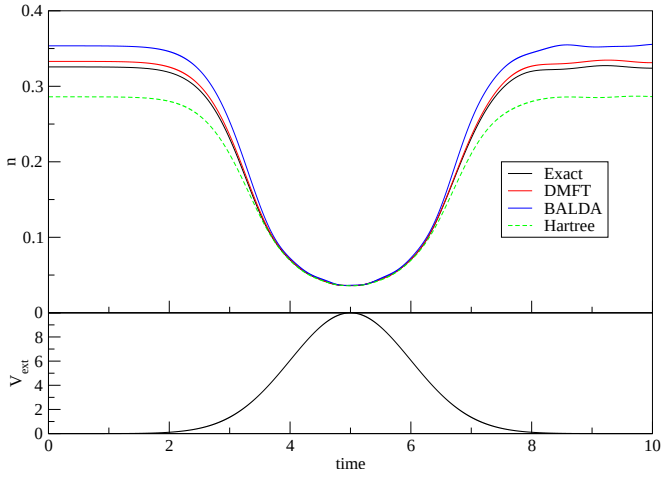

Figure 3.13: *The potential is now a Gaussian,* $V_{ext}(\tau) = 10 \exp\left(-(\tau - 5)^2/2\right), U = 8, E = 0$.

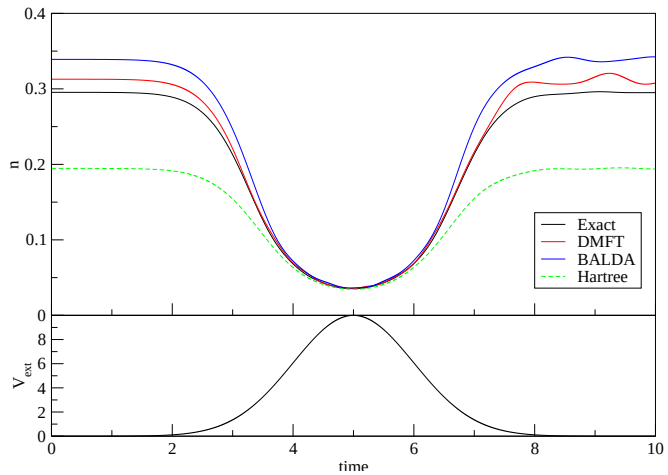

Figure 3.14: *Same as in 3.13 but with a stronger particle interaction,* $U = 24$.

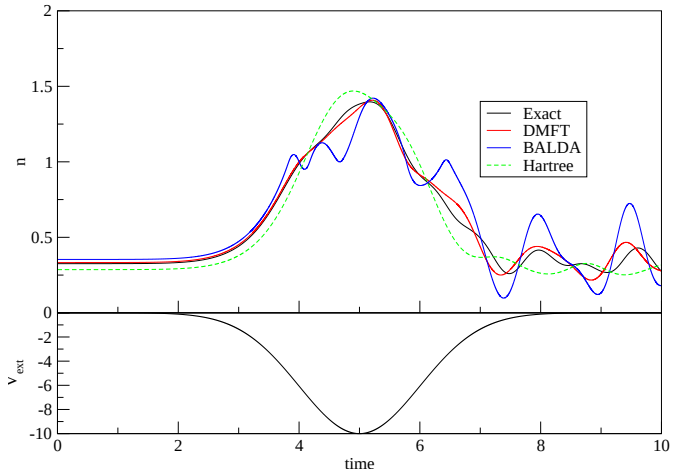

Figure 3.15: *The potential is a gaussian,* $V_{ext}(\tau) = -10 \exp\left(-(\tau - 5)^2/2\right)$. *The interaction strength is* $U = 8$ *and the on-site energy* $E = 0$.

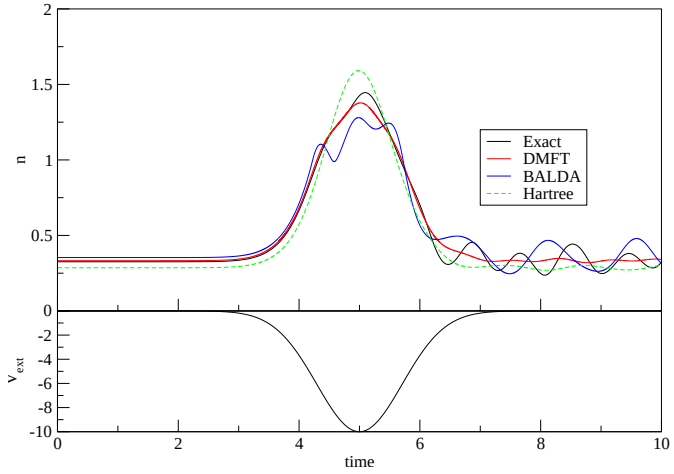

Figure 3.16: *As in 3.15, but with a steeper slope,* $V_{ext}(\tau) = -10 \exp\left(-(\tau - 5)^2/1\right), U = 8$.

and thus the oscillations must be due to the discontinuity in the BALDA potential, see figure 3.7. After the discontinuity has been crossed, the system suddenly gets a large energy penalty, and thus the density tends to decrease. On the other hand, the DMFT potential has no such discontinuity for $U = 8$, and therefore shows no such oscillations around $n = 1$.

In figure 3.16, the perturbation varies faster than in figure 3.15, and after $V_{ext}(\tau) = 0$, the density for the middle site is not in phase with the perturbation. This means that the perturbation is non-adiabatic, and thus time effects such as memory effects become important. The oscillations of the exact solutions, which are due to such memory effects, are reproduced neither by the DMFT or the BALDA solution, because of the adiabatic local density approximation.

In figure 3.17, both the BALDA and the DMFT solution have the same oscillatory behavior, because here both potentials have a discontinuity. The same form of stability around $n = 1$ could be seen in the case of the 1D simulations in figure 3.2 and figure 3.3. This means that we are recovering a behavior analogous to the one observed for the melting of the Mott plateaus in the previous section when dealing with trapped cold fermion atoms.

In figure 3.18, we tried to further smooth both the potentials, to see if the oscillations become smaller. This is indeed the case, the sharp peaks for the BALDA solution are significantly reduced, and are closer to the exact density. This hints that, even if the true v_{xc} for an infinite system has a discontinuity, the true v_{xc} for a finite system might not.

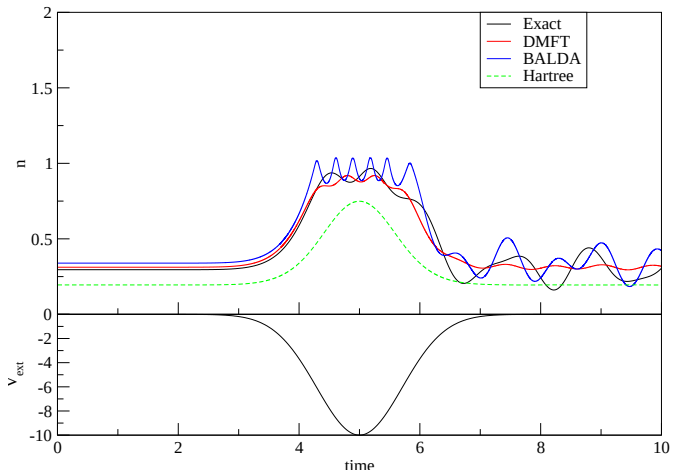

Figure 3.17: *The same as in figure 3.16, but with* $U = 24$.

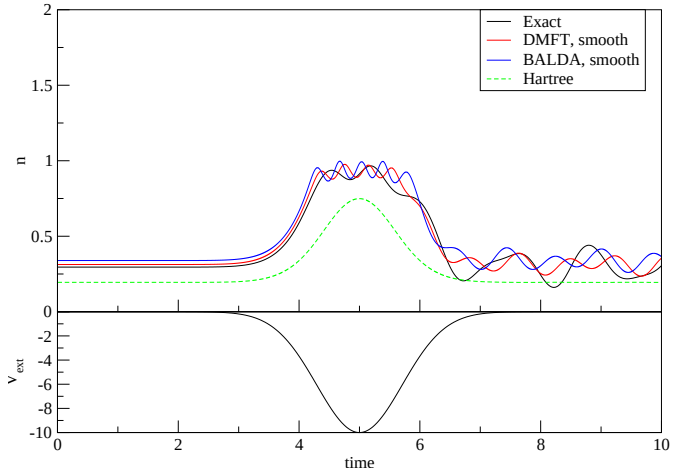

Figure 3.18: *The same as in figure 3.17, but with smoother xc-potentials.*

Larger Clusters

Here, we consider larger clusters than before. We use a simple cubic structure with a size of $5 \times 5 \times 5$ sites with non-periodic boundary conditions, see figure 3.19. There is an on-site particle interaction U on every lattice site in the system, and no on-site energy.

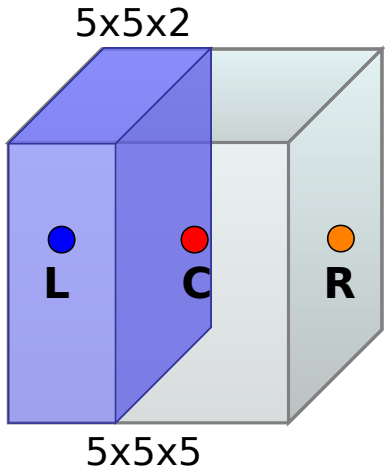

Figure 3.19: *Schematic of the* $5 \times 5 \times 5$ *cube structure. L denotes the site at the center of the left side of the cube, C the center site and R the site on the center of the right side of the cube. The densities for these three sites are shown in the figures below. A time dependent gaussian perturbation is applied to the* $5 \times 5 \times 2$ *sites in the leftmost part of the cube.*

The time dependent perturbation used here is still a gaussian, $V_{ext}(\tau) = A \exp\left(-(\tau - 5)^2/1\right)$, with $A = 2$ or $A = 10$. We apply the perturbation to the 50 sites in the leftmost part of the cube. The electrons will then start to travel from the left side of the cube to the right side. In the figures below we show the densities on the sites furthest to the left (L), in the center (C) and furthest to the right (R).

The total number of electrons will be $N = 70$ or $N = 112$, and the number of spin-up electrons equal the number of spin-down electrons, $N_\uparrow = N_\downarrow$. Note that in a homogeneous cluster with periodic boundary conditions, 70 and 112 correspond to approximately quarter- and half-filling respectively. These numbers were chosen because: i) using 70 electrons the density never crosses half-filling on any of the sites, but it does in the simulations using 112 electrons, thus allowing us to study the effect of the (smoothed) discontinuities at half-filling ii) the ground state for these number of electrons was found to be non-degenerate, see discussion below.

The purpose of these calculations is to show the difference between the BALDA and DMFT solution. No comparison to an exact calculation is

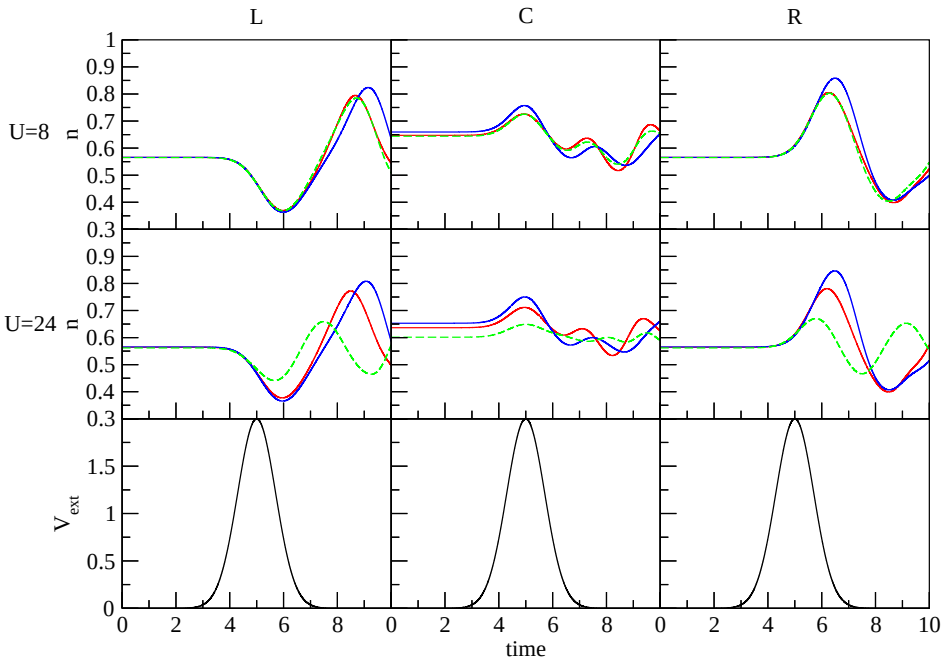

Figure 3.20: *70 electrons, $A = 2$. (L) stands for left, (C) center, (R) right. As before, the red curve corresponds to the DMFT solution, the blue curve to BALDA, and the green curve to the Hartree solution putting $v_{xc} = 0$. The topmost row is for $U = 8$, the middle row is for a stronger particle interaction, $U = 24$. The last row is the external perturbation applied to the left side of the cube.*

made, since the size of such a configuration space is $\binom{125}{35}^2 \sim 10^{62}$.

In figure 3.20 the density is below half-filling. For the purposes of the following qualitative discussion, it is enough to show the results for the densities at the three specific sites displayed in figure 3.19. We have also analyzed the density at other sites, and observed similar behavior. In the beginning of the simulation, the density at L and R are equal, because of symmetry. When the perturbation is applied, the electrons start to move from the left side of the cube to the right, and one can see that at first the density at L goes down, and after a while the density at R goes up. At this time, there is no external potential, and thus the electrons should continue to oscillate back and forth. However, we have not confirmed this numerically. The DMFT and the BALDA solutions have somewhat different behaviors. For $U = 8$, Hartree and DMFT are in close agreement on the L and R sites (but a noticeable disagreement occurs at the central site). On the other hand, while maintaining overall a similar temporal shape, the BALDA curve is rather different from the DMFT and Hartree ones. For $U = 24$, the differences are more enhanced, and now the Hartree solution is no longer close to either BALDA or DMFT.

In figure 3.21 we increase the number of electrons to 112 in order to make the density to cross the half-filling value. Just like in figure 3.20, the electrons go from the left side to the right side. However, when the density crosses half-filling in the middle, the characteristic oscillations for the BALDA occurs, just as in the cold atoms simulations. These oscillations then propagate across the cube. Everytime the density crosses half-filling, on any site, these characteristic oscillations will emerge. No such oscillations are seen for DMFT at $U = 8$, because the potential is continuous. When $U = 24$, the DMFT potential also has a discontinuity, and therefore one can see some oscillations for the 3D DMFT solution too, although not as strong as for the BALDA.

In figure 3.22 the size of the perturbation was increased from $A = 2$ to $A = 10$. For $U = 8$, all three curves exhibit the same behavior. However, for a stronger interparticle interaction $U = 24$, the solutions differ more.

In figure 3.23, since the BALDA density crosses half-filling, the same oscillatory behavior as in 3.21 is observed.

As a conclusive remark, the single feature which has most effect on the BALDA and DMFT time evolution is the discontinuity in the xc-potential. This also applies to the smoothened versions of the v_{xc}. Nevertheless, even if neither BALDA nor DMFT densities cross half-filling, the quantitative difference between the two xc-potentials (especially for densities close to half-filling) can cause the solutions to differ noticeably, while an overall resemblance is retained.

On the contrary, when the BALDA or DMFT (or both) densities cross half-filling, we have another kind of behavior: every sudden change in v_{xc} (due to the discontinuity) has a rather dramatic effect on the dynamics. Since the jumps in the DMFT and BALDA potentials do not occur at the exact same time (even if they occurred at the same time, the size of the discontinuity would be different), any jump across the half-filling (at any site in the system) will increase the discrepancy between the two trajectories. Such behavior will begin to manifest after the first jump. It is expected that the discrepancy between BALDA and DMFT will increase in time, especially if the densities cross half-filling several times, due to the cumulative effect of many jumps.

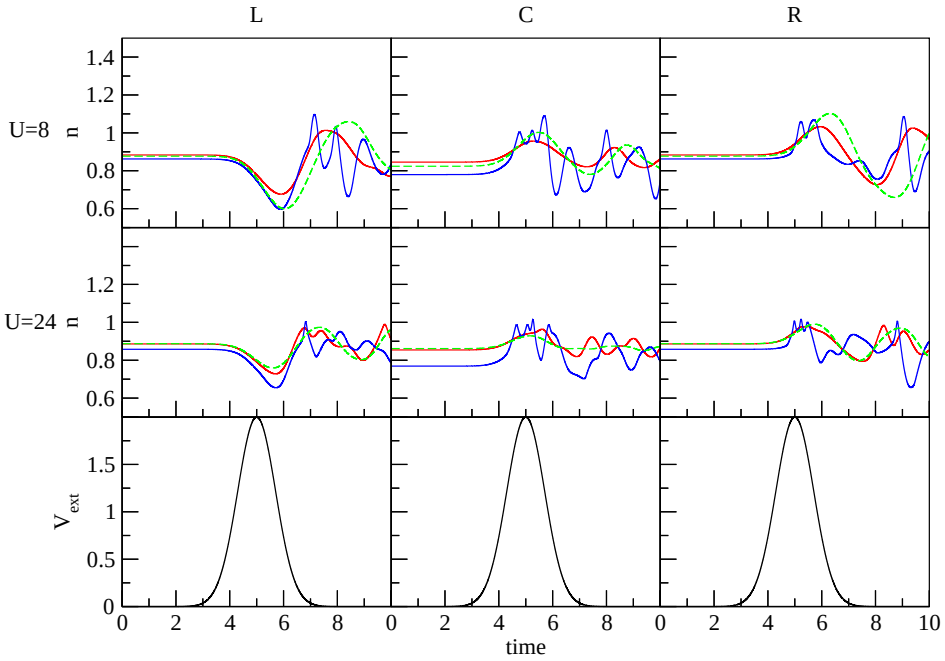

Figure 3.21: *112 electrons, $A = 2$. Red: DMFT, blue: BALDA, green: Hartree.*

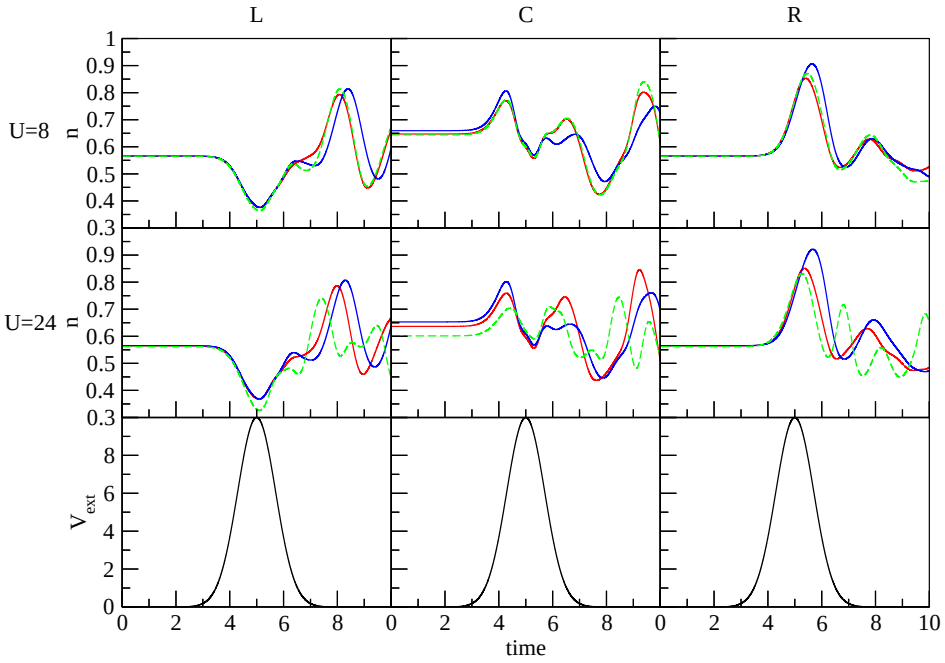

Figure 3.22: *70 electrons, $A = 10$. Red: DMFT, blue: BALDA, green: Hartree.*

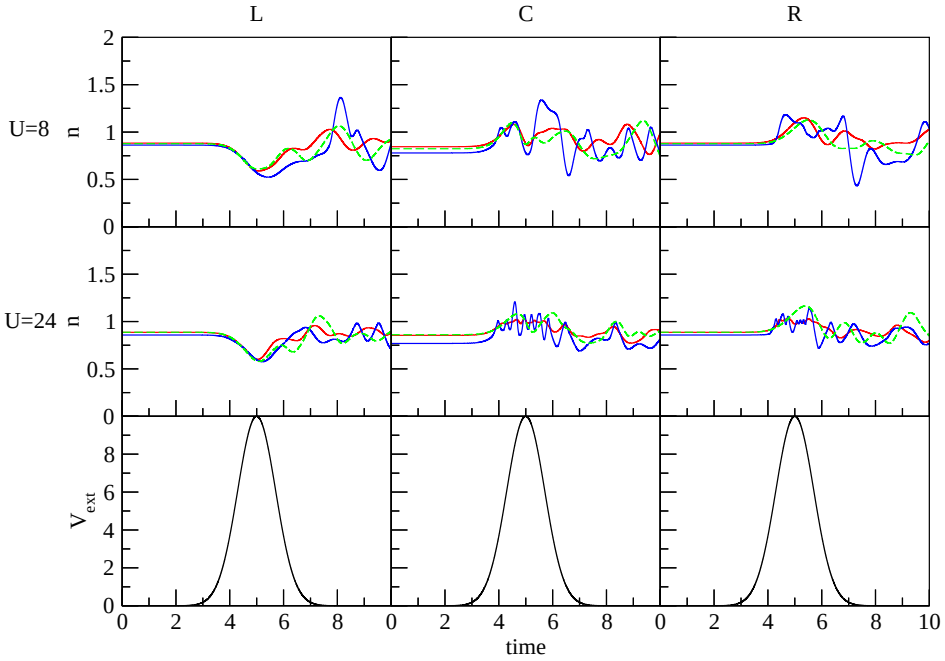

Figure 3.23: *112 electrons, $A = 10$. Red: DMFT, blue: BALDA, green: Hartree.*

3.3.3 Note about degeneracies

We would like to make here some observations about the exact and TDDFT solutions in the 19-site cluster. A 19 site cubic cluster with one impurity in the middle has many symmetries, which means that often the ground state is degenerate; there exists Kohn-Sham orbitals at the Fermi energy with the same energy. If the degeneracy is below the Fermi energy, this will not affect anything. This is also true if degeneracies are above the Fermi energy. The crucial part is when the Fermi energy is equal to the degenerate energy levels.

This is not a problem in the ground state calculations. For a non-degenerate system, the many-body ground state is constructed by filling the Kohn-Sham orbitals from the bottom up, the orbitals corresponding to the lowest eigenvalues are filled first. For the degenerate case, one can imagine that the degenerate states are filled evenly, which implies an average sum of the Kohn-Sham orbitals absolute squared. In this way one gets a consistent ground state density.

However, to do a time dependent calculation one needs to evolve a specific initial unique state, and this can be problematic in case of degeneracy. A possible way out of this drawback is to adopt one of the following two procedures:

1. Only time evolve systems which have such a number of electrons that the degenerate levels are filled, and the next empty state is non-degenerate.

2. Change the system in such a way that the symmetry is reduced, thus lowering the number of degenerate states.

Since, for the exact calculations, one is constrained at present to a maximum of 6 electrons, 1) cannot be easily used. Therefore, route 2) was used there. This consisted of adding some disorder to the system by adding small values of on-site energies to specific sites, on the order of $v_i \sim 0.01$. This removed the low lying degeneracies.

Note that, however, for the $5 \times 5 \times 5$ calculations, where no exact simulations were made, we resorted to method 1).

Chapter 4

Conclusions and outlook

In this work, we have used the TDDFT approach to i) investigate the behavior of cold fermion atoms trapped in 1D optical lattices and ii) propose a new way to describe the behavior of strongly correlated systems in 3D. For i), we have applied a pre-existing DFT and TDDFT scheme for the 1D Hubbard model to study the dynamical melting of a Mott insulator for a system of fermions trapped in a parabolic trap.

We have seen that different regions of the system in the ground state evolve differently in time when the parabolic potential is removed. The band insulator region collapses immediately, while the Mott plateaus are much more stable against the change in potential. This means that the electron-electron interaction stabilizes the Mott region. A paper that reports the results of these investigations has been recently submitted for publication, see [18].

To pursue part ii), we have used Dynamical Mean Field Theory to generate an exchange-correlation potential suitable for the Hubbard model in 3D. We have also compared the time dependent DMFT solution to the BALDA one for 3D structures, and we saw that for densities not crossing half-filling, both the DMFT and BALDA do a relatively good job. However, as expected on conceptual grounds, DMFT is better than BALDA.

However, when the half-filling is crossed, the time dependence is radically changed. Here DMFT does a better job than BALDA, especially below the Mott phase transition. This should be attributed to the discontinuity in the V_{xc} which is always present in the 1D BALDA, but not in the 3D DMFT away from the Mott phase, for low values of U. Therefore the two different functionals are expected to produce different behaviors, which they do.

Looking back, we can see that the results are encouraging. This first attempt on a DMFT-based TDDFT approach is seen to capture much of the dynamical behavior of the 3D Hubbard model. The calculation times were feasible, and larger systems can be simulated. Primary tests have shown that

even larger systems than the ones described in this thesis can be simulated. Such systems are impossible to simulate using the exact method employed in this thesis, and thus one can think of resorting to other methods such as for example Quantum Monte Carlo, in order to check the DMFT+TDDFT method.

Nevertheless, the results hint that it is possible to use TDDFT to describe strongly correlated systems, using a DMFT-based functional.

As a conclusive remark, we note that in the second part of this thesis, namely the one devoted to TDDFT+DMFT, the emphasis has been primarily on a technical characterization the new xc-potential. However, among our plans for future research, we mention possible applications to a variety of problems, such as, for example, studies of Bloch oscillations, cold atoms in 3D optical lattices and dynamically pressure-induced metal-insulator transitions.

These future studies, besides addressing interesting physical phenomena, will provide challenging tests to the newly proposed xc-potential. More in general, it will further elucidate the scope of a time dependent density functional theory for strongly correlated systems out of equilibrium, maybe even at the ab-initio level.

Acknowledgements

I would like to thank my supervisor Claudio for everything he has taught me, for all his time, support and, most of all, patience with me during the time I spent at the department. I would also like to thank Carl-Olof for discussions and for proofreading of my thesis, and Ulf for showing interest and encouragement for my work. I am also grateful to the department of mathematical physics, which has provided a pleasant atmosphere to do work in. I also would like to express gratitude to my collaborators outside of Lund University; Klaus Capelle, Mariana M. Odashima and Antonio Privitera. Finally, I am grateful to Ulrika for her never-ending support in everything.

Appendix A

Fitting of the DMFT E_{xc}

The total energies obtained within DMFT consisted of several tables, one for each value of U, of the total energy as a function of density, and the kinetic energy as a function of density, for densities $0 < n < 1$. The exchange-correlation energy as a function of density was constructed by subtracting the kinetic energy and the Hartree energy from the total energy. One could then, in principle, simply take the numerical derivative

$$v_{xc}(n) = \frac{E_{xc}(n + \Delta n) - E_{xc}(n)}{\Delta n} \tag{A.1}$$

and then use the fact that the E_{xc} is symmetric around half-filling, to obtain the potential for $1 < n < 2$. However, this has two limitations: i) the E_{xc} is not very smooth everywhere, especially not for low densities or densities close to half-filling. This noisy behavior can be attributed to the impurity solver in the DMFT code. Thus the v_{xc} will have sharp "spikes" in it. ii) We only obtain a v_{xc} for the data points in the data set, but we need to know v_{xc} everywhere, as a function of the density.

Issue i) can be partially solved by a smoothing procedure. We used a running average procedure for the E_{xc}, until the desired smoothness was achieved. However, the noise for low and half-fillings were not easily removed by this method, see below.

Issue ii) can be solved by fitting functions to the E_{xc}, and then taking the analytical derivative of that function to get the v_{xc}. The fittings were done using the fit-function in GNUplot.

In order to fit a function close to half-filling, were the data was rather noisy, we simply assumed a quadratic behavior for the E_{xc}, which means a linear behavior for the v_{xc}.

For low fillings, we utilized a known fact about the Hubbard model at low fillings. Giuliani [19] has derived an asymptotically correct formula, which describes the total energy for the 3D Hubbard model in the low density limit. From this, one can then extract the exchange-correlation energy as before.

The formula used is

$$E_{xc} = E(n,U) - E_0(n) - Un^2/4 = (8\pi a_s(U) - U)\, n^2/4 \tag{A.2}$$

where a_s is the scattering length for the Hubbard model, given by

$$a_s(U) = \frac{1}{8\pi} \frac{1}{U^{-1} + \gamma} \tag{A.3}$$

where γ depends on the geometry of the system [20]. For a simple cubic lattice, $\gamma = 0.1263t^{-1}$, and thus we have all the ingredients for the low-density formula A.2. One can improve on the asymptotic formula, however, by including the next order term,

$$E_{xc} = (8\pi a_s(U) - U)\, n^2/4 + \beta n^{7/3} \tag{A.4}$$

so that the formula is applicable also for even higher densities. So, for low densities we used the xc-energy from Giuliani's expression instead of the DMFT data.

Now we have an analytical expression both for low densities and close to half-filling (with the linear behavior for the v_{xc}). Since the region in between low and high densities was smooth, we fitted a 5-degree polynomial to the E_{xc}. We tried two other methods: cubic splines, and a Savitzky–Golay smoothing procedure, which gave similar results. However, the polynomial method was deemed to be more smooth and easier to use.

After the polynomial expression for the E_{xc} was obtained, we differentiated it, and then joined the curve to the fittings for the low and half-filling regions. We then obtained an expression for the v_{xc} in the entire range of $0 < n < 2$, and the corresponding exchange-correlation energies and potentials are shown in figure 2.3.

Bibliography

[1] P. Hohenberg and W. Kohn. Inhomogeneous electron gas. *Phys. Rev.*, 136(3B):B864–B871, Nov 1964.

[2] Erich Runge and E. K. U. Gross. Density-functional theory for time-dependent systems. *Phys. Rev. Lett.*, 52(12):997, Mar 1984.

[3] Claudio Verdozzi. Time-dependent density-functional theory and strongly correlated systems: Insight from numerical studies. *Physical Review Letters*, 101(16):166401, 2008.

[4] John P. Perdew, Kieron Burke, and Matthias Ernzerhof. Generalized gradient approximation made simple. *Phys. Rev. Lett.*, 77(18):3865–3868, Oct 1996.

[5] N. A. Lima, M. F. Silva, L. N. Oliveira, and K. Capelle. Density functionals not based on the electron gas: Local-density approximation for a luttinger liquid. *Phys. Rev. Lett.*, 90(14):146402, Apr 2003.

[6] Wei Li, Gao Xianlong, Corinna Kollath, and Marco Polini. Collective excitations in one-dimensional ultracold fermi gases: Comparative study. *Physical Review B (Condensed Matter and Materials Physics)*, 78(19):195109, 2008.

[7] Walter Metzner and Dieter Vollhardt. Correlated lattice fermions in $d = \infty$ dimensions. *Phys. Rev. Lett.*, 62(3):324–327, Jan 1989.

[8] Daniel Karlsson. Bachelor thesis: Studies of time dependent behavior of few interacting electrons in quantum transport geometries, 2008.

[9] Klaus Capelle. A bird's-eye view of density-functional theory, 2002.

[10] Elliott H. Lieb and F. Y. Wu. Absence of mott transition in an exact solution of the short-range, one-band model in one dimension. *Phys. Rev. Lett.*, 20(25):1445–1448, Jun 1968.

[11] Gabriel Kotliar and Dieter Vollhardt. Strongly correlated materials: Insights from dynamical mean-field theory. *Physics Today*, 57(3):53–59, 2004.

[12] Antoine Georges, Gabriel Kotliar, Werner Krauth, and Marcelo J. Rozenberg. Dynamical mean-field theory of strongly correlated fermion systems and the limit of infinite dimensions. *Rev. Mod. Phys.*, 68(1):13, Jan 1996.

[13] Antoine Georges and Gabriel Kotliar. Hubbard model in infinite dimensions. *Phys. Rev. B*, 45(12):6479–6483, Mar 1992.

[14] *Electronic Structure: Basic Theory and Practical Methods: Basic Theory and Practical Density Functional Approaches Vol 1.* Cambridge University Press, 2004.

[15] R. Jördens, N. Strohmaier, K. Günter, H. Moritz, and T. Esslinger. A mott insulator of fermionic atoms in an optical lattice. *Nature* **455** *204*, 2008.

[16] U. Schneider, L. Hackermuller, S. Will, Th. Best, I. Bloch, T. A. Costi, R. W. Helmes, D. Rasch, and A. Rosch. Metallic and Insulating Phases of Repulsively Interacting Fermions in a 3D Optical Lattice. *Science*, 322(5907):1520–1525, 2008.

[17] Gabriele Giuliani and Giovanni Vignale. *Quantum Theory of the Electron Liquid.* Cambridge University Press, 2008.

[18] Daniel Karlsson, Claudio Verdozzi, Mariana M. Odashima, and Klaus Capelle. Dynamical melting of the mott insulator: Time evolution of the density and entropy of out-of-equilibrium cold fermion gases, arxiv:0905.1398v1, 2009.

[19] Alessandro Giuliani. Ground state energy of the low density hubbard model: An upper bound. *Journal of Mathematical Physics*, 48(2):023302, 2007.

[20] Antonio Privitera. Ph.d. thesis. Unpublished.